

Rotating Spherical Interlayer (RSI) Measurement of the Dynamic Mechanical Properties of Elastomers

D. H. KAELEBLE,* *Central Research Laboratories,
3M Company, St. Paul, Minnesota*

Synopsis

An analysis of simple shear in a rotating spherical interlayer is presented. The theory provides design criteria and operating equations for a new method of measuring the dynamic mechanical properties of soft viscoelastic polymers. The storage component of the dynamic shear modulus $G'(\omega) = 3F_1hm^2/2\pi r^4(3 \sin \phi + \sin^3\phi) (\Delta X_t - K_1F_1)$ and the loss tangent $\tan \delta = [F_2(\Delta X_t - K_1F_1) - K_2F_1F_2]/[F_1(\Delta X_t - K_1F_1) - K_2(F_2)^2]$ are expressed in terms of the inner radius r , thickness h , and arc angle ϕ of sample extending from the rotational equator; the biaxial dynamometer compliances K_1 , K_2 ; the imposed dynamometer displacement ΔX_t ; and the spherical interlayer storage and loss forces F_1 , F_2 . New instrumentation involving a rotating spherical interlayer (RSI) transducer and a rotational accessory to the Instron provides measurements from 0.001 to 45 cycle/sec at temperatures from -50° to 200°C . A comparison of RSI data, treated by time-temperature superposition, and literature values of dynamic response in polyisobutylene confirms both theory and method.

INTRODUCTION

Two versatile techniques for measuring the dynamic mechanical properties of plastics have been reported by Maxwell.^{1,2} Both methods utilize the flexure of a rotating cantilever beam in the form of a circular plastic rod to measure the storage and loss components of the dynamic Young's modulus. This measurement technique, being a direct stress-strain method, provides a broad and continuously variable frequency range under conditions of either constant dynamic stress¹ or strain.² A recent theoretical analysis defines the constant stress or constant strain methods as limits of the actual intermediate stress-strain state in the material and defines the measurement in terms of new operating equations.³

The conventional rotating cantilever beam measurement is normally limited to rods of plastic or highly crosslinked elastomer whose dynamic Young's modulus is greater than $E^*(\omega) = 1.10^8$ dyne/cm².^{1,2,4} This limitation created an interest in extending the principles of rotational dynamic measurement to softer materials. The objective was the retention of the basic simplicity and flexibility of the Maxwell instrument combined with the new capability of measuring dynamic shear properties of elasto-

* Present address: Science Center/Aerospace and Systems Group, North American Rockwell Corporation, Thousand Oaks, California 91360.

mers in both the rubbery plateau and flow regions of viscoelastic response. Consideration of various geometries of deformation quickly led to the conclusion that simple shear in a spherical plane provided the suitable means of accomplishing the desired result.

This article presents the extension of the theory of rotational dynamic measurement to treat rotational deformation of a spherical interlayer in simple shear. A description of new instrumentation for conducting both cantilever beam and spherical interlayer measurements is also presented.

THEORY OF OPERATION

This analysis treats the limiting case of shear in a thin interlayer which is bonded to a concentric ball and socket transducer of the type schematically presented in Figure 1. The RSI transducer shown in this illustration presents two end geometries, one for clamping in the rotating spindle, the other for rolling contact with a biaxial dynamometer. These end geometries are analogous to the circular beam geometry of a Maxwell specimen.

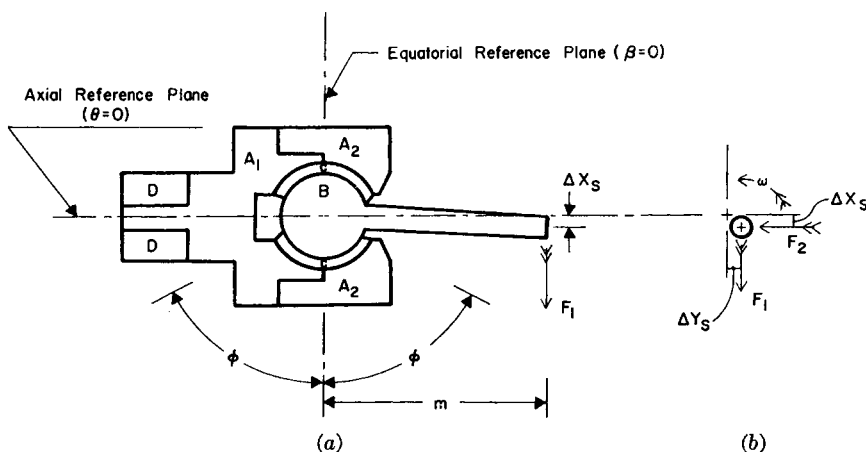


Fig. 1. Full cross-section axial view (A) and moment arm end view (B) of the RSI transducer: A_1 , A_2 , separable parts of a spherical socket; B , spherical ball and moment arm; C , spherical interlayer sample deformed in shear; D , collet chuck for attaching the transducer; 2ϕ , arc angle of sample interlayer centered at the rotational equator; ω , rotational frequency about the line of centers of parts A , B , and D ; m , moment arm of forces F_1 and F_2 about the spherical center of rotation; F_1 , F_2 , perpendicular external forces; ΔX_s , ΔT_s , perpendicular deflections associated respectively with F_1 and F_2 .

In fact, the RSI transducer is interchangeable with a Maxwell-type specimen and basically the same instrument can perform both types of measurement. The function of the RSI transducer is to transform a deflection in the axis of free rotation of part B into a cyclic shearing of the material within the spherical gap between the concentric ball and socket. This deflection is applied at the end of the moment arm of the ball by the previously described rolling contact between closely spaced ball bearings.^{1,2}

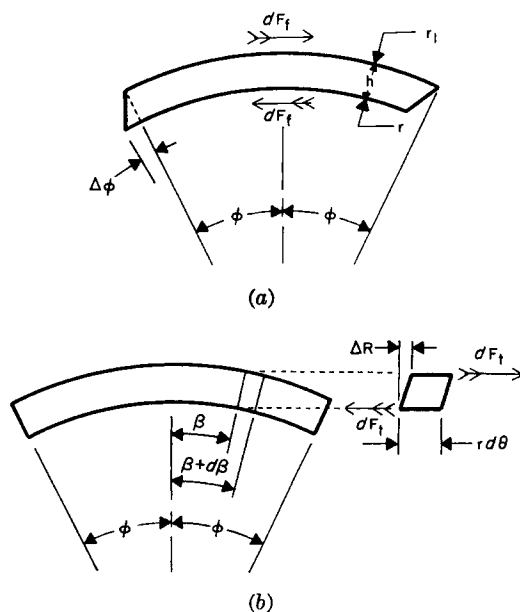


Fig. 2. (A) Geometry of simple shear in an incremental $d\theta$ element of the spherical plane: r, r_1 , respective radii of ball and socket; h , interlayer thickness; $\Delta\phi$, shear displacement; f , shear force. (B) Geometry of torsional shear in an infinitesimal $d\theta d\beta$ element of the spherical plane: β , arc angle from the equatorial plane; ΔR , torsional shear displacement; t , torsional shear force.

These bearings are presumed frictionless and therefore apply no reverse torque to the rotating moment arm.

Figure 1A shows the RSI transducer in a condition of static deflection between the ball and socket. The deflection ΔX_s , at a distance m along the moment arm is accomplished by an external force F_1 . This external moment of force $F_1 m$ is in equilibrium with a reactive moment of force provided by the deformed sample. This first part of the discussion will define the sample deformation for the static case. Two schematics are required to describe this sample deformation. Figures 2A and 2B present the two modes of shear deformation which arise.

In order to visualize the deformations depicted in Figure 2, it is necessary to construct two planes of orientation in Figure 1A. The first of these reference planes is the equatorial plane of rotation of the socket (part A). The edge view of this equatorial plane coincides with the vertical center line of Figure 1A where the arc angle $\phi = 0$. The second plane of orientation is axial and is represented in edge view by the horizontal center line of Figure 1A. The full cross section presented in Figure 1A is provided by the rotation of this axial reference plane by an angle $\theta = \pi/2$ to provide the vertical cross section.

The sample C of Figure 1A is symmetrically disposed over an arc angle of 2ϕ about the equatorial plane of the transducer. A static deflection

ΔX_s at a distance m produces a maximum amplitude of simple shear deformation in the axial plane represented by $\theta = \pm \pi/2$. This simple shear deformation is represented by the cross section of the spherical interlayer shown in Figure 2A. In the axial plane $\theta = 0$, or the horizontal axial plane, this simple shear mode disappears and is replaced by a more complicated mode of deformation—shown in Figure 2B. This second mode of deformation is termed torsional shearing and increases in proportion to the arc angle β from the equatorial plane. This torsional mode of shear has a maximum amplitude in the axial plane $\theta = 0$ and disappears when $\theta = \pm \pi/2$. This analysis thus must account for the integrated resultant of these two modes of shear over the spherical area of contact provided by the sample between the ball and socket. It is assumed in this simplified derivation that the interlayer thickness h is very small compared to the respective radii r and r_1 of the ball and socket such that shear strain is uniform through the sample thickness.

Treating the simple shear mechanism shown in Figure 2A, it may be seen that the shear strain γ may be expressed as follows:

$$\gamma = \frac{r\Delta\phi}{h} = \frac{r\Delta X_s \cos \phi}{hm} \quad (1)$$

where the displacement angle $\Delta\phi = (\Delta X_s \cos \theta)/m$ and the interlayer thickness $h = r_1 - r$. The shear stress s is given by the geometry of Figure 2A and is

$$s = \frac{dF_f}{2r^2 \sin \phi d\theta} \quad (2)$$

From the standard relation for shear modulus $G = s/\gamma$ it follows from eqs. (1) and (2) that

$$dF_f = \frac{2Gr^2\Delta X_s \sin \phi \cos \theta d\theta}{hm} \quad (3)$$

Since the effective moment arm of force dF_f is its displacement from the axial plane $\theta = \pi/2$, it follows the incremental moment of force $dM_f = r \cos \theta dF_f$. The interrelation which expresses the necessary condition of equilibrium between the external and internal moments of force may be written as follows:

$$F_f \cdot m = 4 \int_{\theta=0}^{\pi/2} dM_f = \frac{8Gr^4 \sin \phi \Delta X_s}{hm} \int_0^{\pi/2} \cos^2 \theta d\theta$$

which upon integration becomes

$$F_f = \frac{2\pi Gr^4 \sin \phi \Delta X_s}{hm^2} \quad (4)$$

where F_f is the total external force at moment arm m due to the simple shear mode of sample deformation.

The torsional mode presented in Figure 2B is equivalently treated, and from this schematic the shear displacement ΔR is seen to be

$$\Delta R = \frac{r\Delta X_s \sin \beta \sin \theta}{m}. \quad (5)$$

The shear strain γ for the incremental volume $h \cos \beta d\beta d\theta$ is

$$\gamma = \frac{\Delta R}{h} = \frac{r\Delta X_s \sin \beta \sin \theta}{mh} \quad (6)$$

The shear stress s for this mode is by inspection of Figure 2B seen to be

$$s = \frac{dF_t}{r^2 \cos \beta d\beta d\epsilon}. \quad (7)$$

From the relation for shear modulus $G = S/\gamma$ we may combine eqs. (6) and (7) and with rearrangement write the following expression for shear force due to torsion:

$$dF_t = \frac{r^3 G \Delta X_s \sin \theta \sin \beta \cos \beta d\theta d\beta}{mh}. \quad (8)$$

Recognizing the effective component of the shear force dF_t to be the component projecting in the direction parallel to the axial plane $\theta = \pi/2$, it follows that the effective torsional shear force is $dF_t \sin \theta$. Correspondingly the effective moment arm of this force is $r \sin \beta$. The infinitesimal moment of the torsional deformation is $dM_t = r \sin \theta \sin \beta dF_t$, which upon substitution into eq. (8) becomes

$$dM_t = \frac{r^4 G \Delta X_s \sin^2 \theta \sin^2 \beta \cos \beta d\theta d\beta}{mh}. \quad (9)$$

By writing the expression for equilibrium of the external force and internal moments of the torsional deformation, the following expression results:

$$F_t \cdot m = 4 \int_{\beta=0}^{\pi/2} 2 \int_{\theta=0}^{\phi} dM_t = \frac{8r^4 G \Delta X_s}{mh} \int_0^{\pi/2} \int_0^{\phi} \sin^2 \theta \sin^2 \beta \cos \beta d\theta d\beta$$

which upon integration and rearrangement provides the desired expression for the external force:

$$F_t = \frac{2\pi \Delta X_s G r^4 \sin^3 \phi}{3m^2 h} \quad (10)$$

where F_t is the total external force at moment arm m due to the internal torsional deformation.

For the static case the expression for the total force F_1 depicted in Figure 1A is thus the sum of the shear and torsional forces. Summing eq. (5) and eq. (10) provides the following expression:

$$F_1 = F_f + F_t = \frac{2\pi G r^4 \Delta X_s}{3hm^2} (3 \sin \phi + \sin^3 \phi). \quad (11)$$

Equation (11) may be applied directly to the dynamic case of rotational shear at rotational frequency ω by the substitution of the dynamic storage modulus $G'(\omega)$ for the static modulus G . Since one dynamic cycle of shear strain is imposed on the interlayer for each revolution of the RSI transducer, the rotational and cyclic dynamic frequencies are synonymous.

As was previously the case in the development of operating equations for rotating cantilever beam measurement,³ it is necessary to consider a finite instrument compliance in both the x and y axis indicated in Figure 1B. A treatment of this interaction of the biaxial dynamometer and the RSI transducer exactly parallels that provided previously for the cantilever beam-type sample. Applying these relations to the case presented here, we find for the x axis in which imposed strain is applied that

$$\Delta X_s = \Delta X_t - K_1 F_1 \quad (12)$$

where ΔX_t is the total dynamometer deflection and K_1 is the x -axis spring constant of the dynamometer. Substituting eq. (12) and the storage modulus $G'(\omega)$ for G into eq. (11) provides, with rearrangement, the following relation:

$$G'(\omega) = \frac{3hm^2}{2\pi r^4 (3 \sin \phi + \sin^3 \phi)} \frac{F_1}{(\Delta X_t - K_1 F_1)}. \quad (13)$$

Equation (13) thus permits direct calculation of the storage modulus $G'(\omega)$ at frequency ω by measurements of ΔX_t and F_1 .

Under a condition of dynamic deformation the viscoelastic material in the RSI transducer will display a viscous component of shear stress which is out of phase with the storage or reversible elastic stress. This viscous response is defined in terms of a phase angle δ between dynamic stress and strain whose tangent is defined by the ratio

$$\tan \delta = \frac{G''(\omega)}{G'(\omega)} \quad (14)$$

where $G''(\omega)$ is the loss modulus at frequency ω . Under sinusoidal deformation in forced vibration, the stress wave in a viscoelastic material always leads the strain wave by the phase angle δ . In the rotational case this leads to the neutral axis of stress by an arc angle which equals the phase angle δ . Figure 3 depicts end view cross sections of the loading point (in the left column) and the equatorial plane of rotation (two central columns) of the RSI transducer.

Three conditions of external loading are described in Figure 3. The constant stress condition describes the application of a force F_1 with free deflection of the moment arm m to displacements ΔX_s and ΔY_s . The orientation of the neutral axes, where both shear stress and strain are zero, is indicated for both the shear mode and torsion mode of interlayer deformation. It may be noted that both the shear and torsion mode display the same phase angle δ , but their neutral axes are rotated with respect to each other by an angle $\pi/2$.

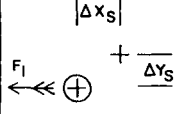
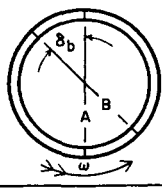
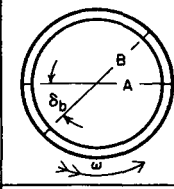
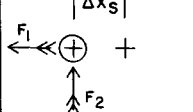
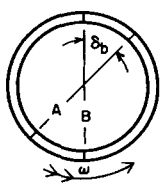
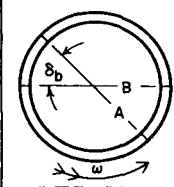
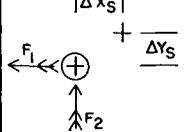
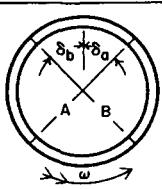
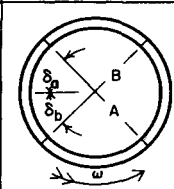
EXTERNAL FORCE AND DISPLACEMENT AT DISTANCE m	SHEAR MODE STRESS & STRAIN IN RSI	TORSION MODE STRESS & STRAIN IN RSI	DEFINING RELATION
CONSTANT STRESS 			$\tan \delta_b = \frac{\Delta Y_s}{\Delta X_s}$ $= \frac{G''(\omega)}{G'(\omega)}$
CONSTANT STRAIN 			$\tan \delta_a = \frac{P_2}{P_1}$ $= \frac{G''(\omega)}{G'(\omega)}$
COMBINED CONSTRAINTS 			$\tan \delta = \tan (\delta_a + \delta_b)$ $= \frac{G''(\omega)}{G'(\omega)}$

Fig. 3 Geometry of external and internal stress and strain: δ_a , phase angle under constant strain; δ_b , phase angle under constant stress; A, neutral axis of internal stress; B, neutral axis of internal strain.

The constant strain condition of deformation shown in Figure 3 occurs where a deflection ΔX_s is imposed with the consequent development of equilibrium forces F_1 and F_2 . This constant strain condition may be obtained only if the dynamometer required to measure F_1 and F_2 displays infinite stiffness. The neutral axis of the shear and torsion modes are rotated with respect to those shown for constant stress due to the differing external force and displacement.

A third condition, described as combined constraints, is depicted in the bottom row of Figure 3. This condition is a composite of constant stress and constant strain and is the normally obtained response when a biaxial dynamometer is employed to impose deflection and measure response. Since a deflection is imposed on the transducer moment arm in the x axis only, the transducer deflection ΔY_s is equivalent to the dynamometer deflection ΔY_c . This interaction may be stated as follows:

$$\Delta Y_s = \Delta Y_c = K_2 F_2 \quad (15)$$

where K_2 is the y axis compliance of the dynamometer. By utilizing the relations for $\tan \delta$ provided in Figure 3 it is evident that

$$\tan \delta = \frac{\tan \delta_a + \tan \delta_b}{1 - \tan \delta_a \tan \delta_b} = \frac{F_2 \Delta X_s + F_1 \Delta Y_s}{F_1 \Delta X_s - F_2 \Delta Y_s} \quad (16)$$

Substituting eq. (12) and eq. (15) for the ΔX_s and ΔY_s terms of eq. (16) provides the desired equation for the loss tangent:

$$\tan \delta = \frac{F_2(\Delta X_t - F_1 F_1) - K_2 F_1 F_2}{F_2(\Delta X_t - K_1 F_1) - K_2 (F_2)^2}. \quad (17)$$

Equation (17) is identical with the previously derived equation for the loss tangent of a Maxwell-type rotating beam specimen.³

From these two basic relations for the RSI transducer, namely eq. (13) and eq. (17), the remaining dynamic mechanical properties of a linearly viscoelastic material may be defined as follows:

$$G''(\omega) = G'(\omega) \tan \delta \quad (18)$$

$$|G^*(\omega)| = [(G')^2 + (G'')^2]^{1/2}. \quad (19)$$

Equation (18) is, of course, a restatement of eq. (14) in terms of the loss modulus $G''(\omega)$. Equation (19) is the conventional expression for the absolute value of the complex shear modulus $|G^*(\omega)|$ at frequency ω .

The development of the RSI theory of operation has pointed to the fact that the extremes of constant stress or constant strain-type dynamic deformation may be obtained by variation in the instrument compliances K_1 and K_2 . The criteria for approaching either type of deformation have been previously described³ for the Maxwell-type specimen. Similar criteria are applicable in the RSI transducer measurement. It is of interest to restate these criteria for the RSI case in order to compare the instrument design factors for the two types of measurement. The instrument design criteria for both the RSI and Maxwell-type measurements are summarized in Table I. In general, the D value described in Table I for the two types of

TABLE I
Criteria for Constant Stress or Constant Strain Dynamic Measurement

Measurement condition	Prerequisite to condition fulfillment within 1% precision	Associated instrument design criteria ^a
Constant stress		
storage modulus	$d(\Delta X_s)/d(\Delta X_t) \geq 100$	$K_1 \geq 100 D$
loss tangent	$\tan \delta_b / \tan \delta_a \geq 100$	$K_2 \geq 100 D$
Constant strain		
storage modulus	$d(\Delta X_s)/d(\Delta X_t) \leq 0.01$	$K_1 \leq 0.01 D$
loss tangent	$\tan \delta_b / \tan \delta_a \leq 0.01$	$K_2 \leq 0.01 D$

^a For RSI transducer $D = 3hm^2/\pi r^2 2(3 \sin \phi + \sin^3 \phi) G'(\omega)$; for maxwell-type specimen $D = 64L^3/3\pi d^4 E'(\omega)$; where L = cantilever beam length, d = diameter of circular beam, and $E'(\omega)$ = tensional storage modulus.

measurement is much lower for the RSI transducer than for the typical Maxwell specimen. This fact requires substantially lower values of instrument compliance $K_1 \simeq K_2$ for the RSI measurement in order to obtain the preferred constant strain-type dynamic deformation.

THE RSI TRANSDUCER AND SAMPLE

An RSI transducer of the type depicted in Figure 1A was constructed for initial experimental studies. Figure 4 provides a photographic view of the transducer and sample in partial state of dismantling pursuant to completion of measurements. Figure 4 shows parts A₁ and B of the transducer clamped in an aligning jig with part A₂ resting in the foreground against the jig. The transducer and sample are normally clamped in the jig except during the measurement.

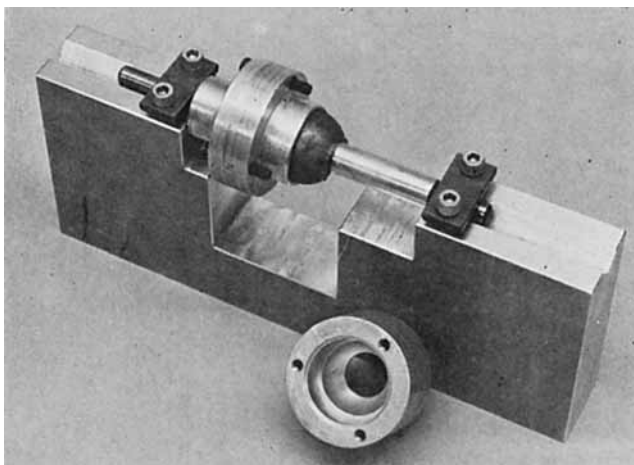
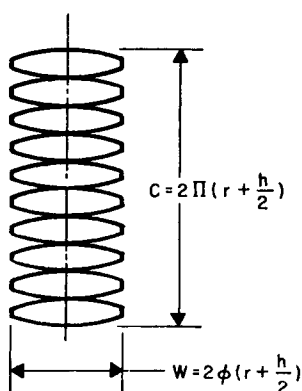


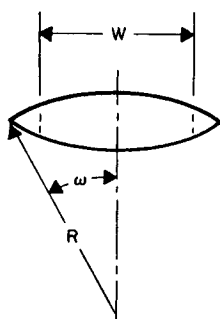
Fig. 4. View of the RSI transducer clamped in its aligning jig with the socket cap (part A₂) removed.

Sample preparation of RSI measurements involves a reverse sequence of these illustrations. Normally a sample is first cast from solution by a special centrifugal casting technique which insures a defect-free film of high thickness uniformity.⁵ The film thickness is controlled so as to exceed the RSI sample thickness h by about 5% in order to insure good interfacial bonding and slight extrusion during assembly of the transducer. This cast film is vacuum dried to remove last traces of solvent, then sandwiched between two thin films of polytetrafluoroethylene (PTFE) to protect the surfaces from contamination.

A pattern of spherical segments as illustrated in Figure 5A is cut from the film. The pattern is a repetition of N single segments whose design is illustrated in Figure 5B. Cutting of the pattern is normally accomplished with the protective films in place. One protective film is then removed and the sample adhered to the cleaned surface of the ball such that the center line of the pattern coincides with the rotational equator of the ball. The outer protective liner is still in place and the socket parts may be employed to gently press the segments into place on the curved surface of the ball. Normally, uncrosslinked elastomers such as polyisobutylene exhibit sufficient compliance and tack to adhere easily under these conditions. At this



(a)



$$\omega = \pi - 2 \operatorname{Arctan} \frac{N}{2}$$

$$R = C / 4 \sin \omega$$

(b)

Fig. 5. Sample pattern (A) and single segment design (B) for the spherical interlayer.

point the outer protective liner on the film is removed and the transducer is assembled, except that the bolts (see Fig. 4) which connect parts A_1 and A_2 (see Fig. 1A) of the socket are left loose. The transducer is clamped in the aligning jig to provide a coaxial condition to the shafts and concentricity to parts A_1 and B. Part A_2 is then drawn into place by tightening the bolts between A_1 and A_2 . Under the pressure provided by closure of parts A_1 and A_2 the segments fuse together and the sample bonds to the surfaces of the ball and socket.

Sufficient time should elapse between this last step of clamping the socket parts and the beginning of dynamic measurements such that appreciable stress relaxation has occurred and the sample-to-transducer interfacial bond is completely established. These conditions of time and temperature may be determined independently by studies of the self-adherence of the sample.⁶ When two parts of the sample are placed in contact, the time-temperature condition which provides an interfacial strength between the parts which is

indistinguishable from their bulk strength denotes the approach to equilibrium bonding and stress relaxation in the transducer.

Following the schematic description of Figure 1A, a typical transducer geometry for measuring elastomer properties in the range $G'(\omega) = 10^5$ to 10^8 dynes/cm² is: $r = 0.375$ in. = 0.95 cm; $h = 0.0625$ in. = 0.159 cm; $m = 2.125$ in. = 5.45 cm; and $\phi = 0.73$ radians. The arc angle ϕ is determined by the sector formed by the spherical geometry of parts A₁ and A₂ of Figure 1A. Material that extrudes out of the spherical interlayer area during bonding is not sheared and does not contribute to the transducer forces P_1 and P_2 . A final check of the adequacy of both cohesive and adhesive bonding of the specimen is, of course, obtained by inspection of the sample after disassembly of the transducer. The illustration of Figure 4 represents a well-bonded specimen.

It should be noted that the transducer depicted in Figures 1 and 4 is merely one example of a number of specialized types that may be designed based upon the theory of RSI operation discussed here. This particular design is interesting for several reasons, which are (1) ease of sample fabrication, (2) freedom from any mechanical support of the ball except through the aligning jig or the sample, and (3) high ratio of m/r to provide for small shear displacements in the sample. Other RSI configurations which provide for pivotal contact between ball and socket at the spherical locus of action permit measurement of dynamic properties of such diverse materials as foamed elastomers, crosslinked elastomers, and completely viscous liquids.

INSTRUMENTATION

In order to obtain a high degree of versatility and precision for rotational dynamic measurement at low cost, the available instrumentation of an Instron Model TT-BM testing machine (Instron Eng. Corp., Canton, Mass.) was employed. Figure 6 presents a photographic view of the Instron equipped with a rotational accessory, mounted on the lower left portion of the machine. A floor-mounted CO₂-air thermostat is shown to the left of the Instron. A Bayley temperature controller rests on the thermostat. To the right of the Instron machine is a rack-mounted Instron integrator and immediately above it, a potentiometer.

Before describing the functions of the auxiliary equipment it is advisable to discuss in more detail the rotational accessory. The frame of this accessory is a short lathe bed that is vertically oriented and bolted to the frame of the Instron. The spindle of the lathe is driven, by means of timing belts, from two alternative shaft positions in the Instron drive system. A high-speed shaft extending from the Instron drive motor provides a spindle speed continuously variable from 44 to 0.5 cycle/sec. A low-speed shaft extending from the Instron transmission box provides two overlapping ranges from 0.5 to 0.01 cycle/sec and 0.05 to 0.001 cycle/sec. The timing belt drive of the rotational accessory is coupled to the Instron drive through magnetic

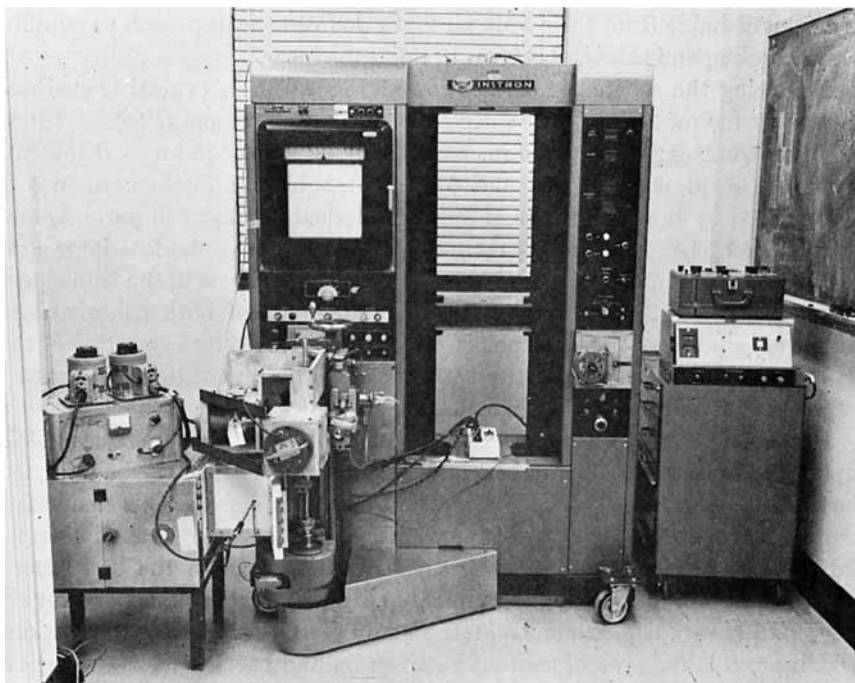


Fig. 6. Instrumentation for RSI transducer measurement of dynamic mechanical properties of polymers.

clutches, thus permitting selection of frequency range or complete disengagement by electrical switching.

Use of the Instron drive system as a frequency generator for the rotational accessory transfers all of the basic features of this positional servo system to control of dynamic measurement. Important among these are synchronously controlled rate, either incremental or continuously variable speed control, and quick reversal of rotation. Using the Instron crosshead as a follower, all of the automatic cycling controls available on the Instron may be transferred to the dynamic measurement.

A second basic feature of the rotational accessory is the biaxial dynamometer. The dynamometer assembly is cantilevered from the upper portion of the lathe bed. This assembly utilizes two Instron load cells mounted in quadrature. The load cells are connected by a yoke arrangement to a vertical tubular column whose lower extremity contains the closely spaced ball bearings through which the forces P_1 and P_2 act upon the sample. Figure 6 presents the view of a regular Maxwell-type specimen which is the deflected rod extending between the spindle collet and the lower extremity of the dynamometer.

Figure 7 presents a view of the dynamometer assembly which shows additional detail of the load cell configuration and the attachment of their load sensing elements to the vertical column. This column, as shown in Fig-

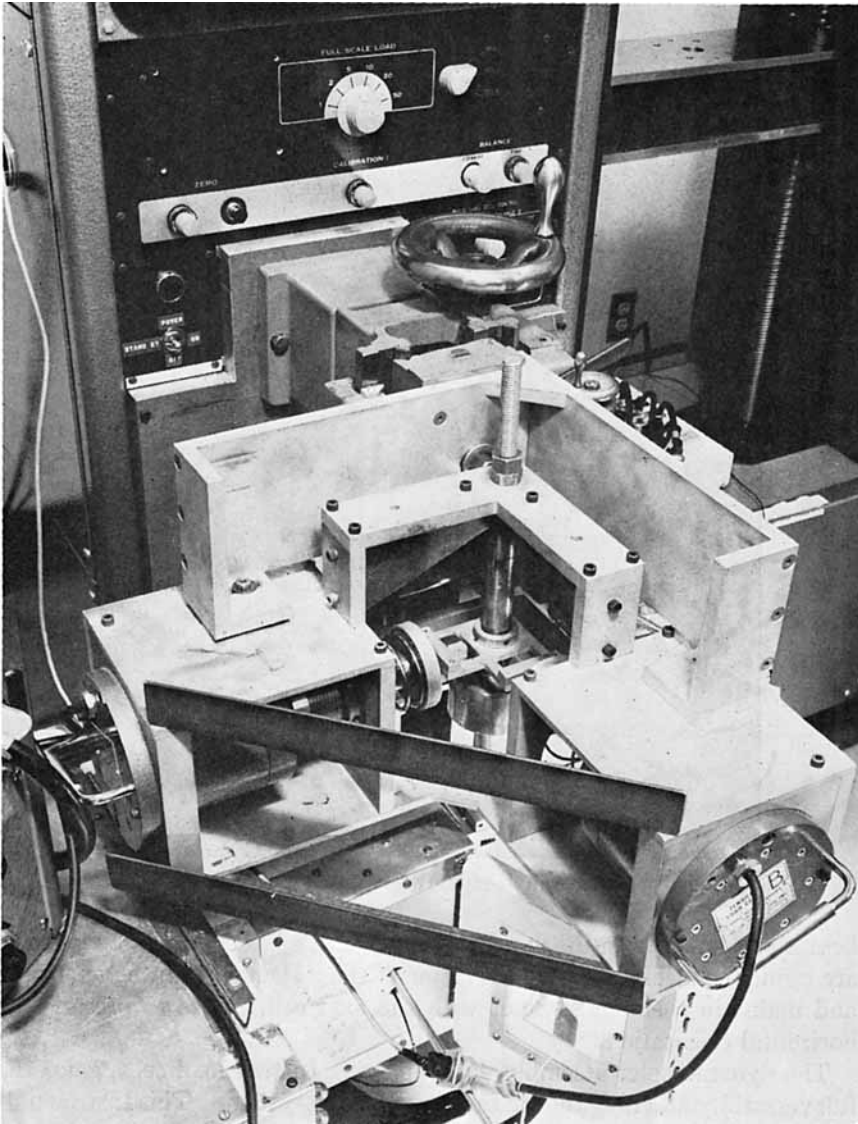


Fig. 7. Close view of the biaxial dynamometer assembly showing load cell configuration.

ure 7, is provided with a heat exchanger immediately below the yoke which connects the load cells. This heat exchanger thermally isolates the load cells and the dynamometer assembly from the lower extremity of the column which is enclosed in the thermostat. The column is constructed of tubular stainless steel to diminish heat flow.

The load cell frame and the top support of the vertical column are one integral unit. This rigid unit translates in both the x and y axes of the horizontal plane. The load cell frame is suspended from the two cantilever

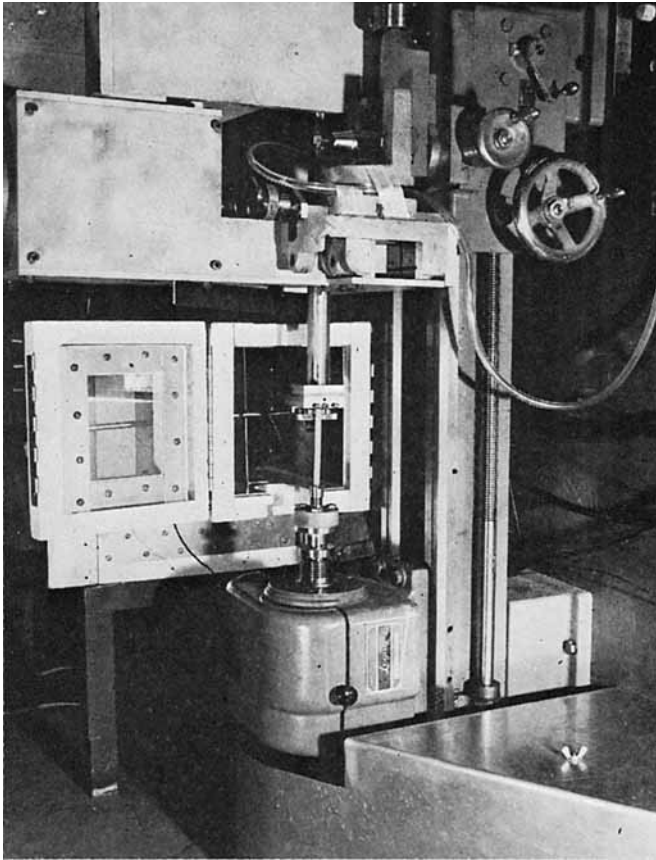


Fig. 8. Close view of the sample-mounting assembly and thermostat enclosure.

beams projecting from the upper extremity of the lathe bed. These beams are rigidly connected to the base frame of the instrument during operation and maintain a sliding contact with the load cell frames to preserve its horizontal orientation.

The dynamometer assembly, by employing Instron load cells, gains the full versatility and range of the Instron weighing system. This Instron unit is equipped with twin bridge calibration circuits to facilitate use of the two force-measuring channels. The Instron integrator is employed to obtain time averaged values of P_1 and P_2 . Both load cells, as shown in Figure 7, are pretensioned to one-half full-load capacity by external compressed coil springs which act in parallel with the force sensing element of each cell. This pretensioning eliminates slack in the flexible linkage connecting the load cell to the vertical beam and permits measurements of positive and negative values of the dynamic forces P_1 and P_2 .

The load cell frame of the dynamometer assembly will accept the full range of Instron cells. The selection of the cell for the x and y axis measurement will depend, of course, on the particular range of forces to be measured

in each axis. The illustration of Figure 7 shows a CM cell (0 to 50 kg range) on the x, or P_1 , axis and a B cell (0 to 2 kg range) on the y, or P_2 , axis. This configuration provides measured values of dynamometer compliances of $K_1 = 0.002 \text{ in./lb} = 1.12 \times 10^{-5} \text{ cm/g}$ and $K_2 = 0.004 \text{ in./lb} = 2.24 \times 10^{-5} \text{ cm/g}$.

The arrangement for enclosing a Maxwell specimen or an RSI transducer in the thermostat is illustrated in the photographic view of Figure 8. The spindle of the drive system terminates in a face plate to which is attached a thermal block composed of fiberglass-reinforced plastic. The sample-collecting fixture is mounted in this block and has no direct metallic contact with the spindle. The thermal block layer rotates in the plane of the lower face of the thermostat. This thermal block in conjunction with the heat transfer unit mounted on the dynamometer provides very effective thermal isolation of the sample from the instrument.

It is of interest here to mention the use of the Bayley controller (Bayley Instrument Co., Danville, Calif.) in obtaining precise temperature control in the recirculating CO_2 -air bath of the thermostat. The Bayley unit, by utilizing a resistance thermometer as one branch of a bridge circuit, senses temperature changes of 0.001°C and provides continuous control to a heating element of up to 500-watt capacity. The standard control circuitry of the thermostat provides a control level of $\pm 1^\circ\text{C}$. The Bayley thermal sensor is placed in the immediate vicinity of the sample and its control circuit modulates the power input to a fast-response free filament heater located in the high velocity region of CO_2 -air flow immediately upstream from the sample. The Bayley unit and filament heater combination form a secondary independent temperature control loop which operates inside the primary $\pm 1^\circ\text{C}$ control cycle. Using this technique, temperature fluctuations are normally less than 0.1°C as measured by thermocouples located on and about the specimen.

This thermostat system provides temperature control from -50°C to 200°C with a precision of 0.1°C through this range. Independent experiments have indicated the importance of properly equilibrating the specimen after arriving at a temperature control point. In our standard operations the sample is rotated continuously under a low deflection force P_1 and at low frequency, normally 0.1 cycle/sec, during temperature change and while thermally equilibrating. This process may be termed dynamic annealing, as it appears to help in preserving circular (in a Maxwell specimen) or spherical (RSI transducer) symmetry of response. In the RSI transducer case a study involving insertion of a thermocouple into the central ball section of the transducer indicated that 30 to 40 min were required to equilibrate this thermally isolated region.

EXPERIMENTAL RESULTS

A sample of NBS polyisobutylene⁷ acquired for an earlier study of creep properties⁸ was utilized in testing the RSI method. This sample has been stored so as to minimize the effects of light and oxidative aging. Intrinsic

viscosity, $[\eta] = 4.49$, was determined in cyclohexane providing a calculated viscosity average molecular weight $\bar{M}_v \simeq 1.1 \times 10^6$ g./mole from the relation of Krigbaum and Flory⁹:

$$[\eta] = 2.6 \times 10^{-4} \bar{M}_v^{0.7}$$

This value compares reasonably well with the value $\bar{M}_v = 1.35 \times 10^6$ g./mole originally reported by Marvin.⁷

A sample was prepared and installed in the RSI transducer by methods described in an earlier section. Measurements were conducted at frequencies from 0.01 to 20 cycles/sec (0.063 to 125.7 rad/sec) at five temperatures. The calculated shear moduli obtained by use of eqs. (13), (17), and (18) were reduced by the temperature ratio $296/T$. Frequencies were reduced to 296°K by the time shift factor a_T through use of the following form of the standard WLF¹⁰ expression:

$$\log a_T = 11.26 - 17.44 \left[\frac{T - T_g}{51.6 + T - T_g} \right]$$

where for polyisobutylene $T_g = 202^\circ\text{K}$. The test conditions of temperature T (°K) and dynamometer deflection ΔX_t are presented in Table II in

TABLE II
Experimental and Superposition Conditions of NBS Polyisobutylene

T, °K	ΔX_t , cm	$\log a_T$ ($T_0 = 296^\circ\text{K}$)	Plot symbol
238.0	0.0254	4.15	○
253.0	0.0152	2.59	◇
273.0	0.0432	1.10	△
296.0	0.0813	0	●
332.0	0.0653	-1.22	▲

conjunction with the frequency shift factor a_T and the plotting symbols employed to construct master curves of the data. The superposed data points of reduced storage G' and loss G'' moduli versus reduced frequency ωa_T are respectively presented in Figures 9 and 10. The solid curves extending through the RSI data represent the dynamic response of this sample as originally reported by Marvin⁷ and slightly shifted from 298°K to reference at $T_0 = 296^\circ\text{K}$.

The data presented in Figures 9 and 10 display a degree of scatter from a smoothed curve which is typical of RSI measurements on other materials. As a comparison between the data and the reference curve indicates, the viscoelastic properties by this recent measurement correlate very closely with earlier work.⁷ Differences in the experimental points and the reference curve may be due to slight aging effects on the sample or simply the manner of data treatment. As noted in Table II, a wide range of ΔX_t was employed in measurement without apparent effect upon either $G'(\omega)$ or $G''(\omega)$ values, thus indicating linear viscoelastic response.

These results strongly attest to the fact that the RSI method provides an accurate means of measuring the dynamic mechanical properties of elastomers. The method is simple and the results may be successfully treated by time-temperature reduced variables. The results presented in

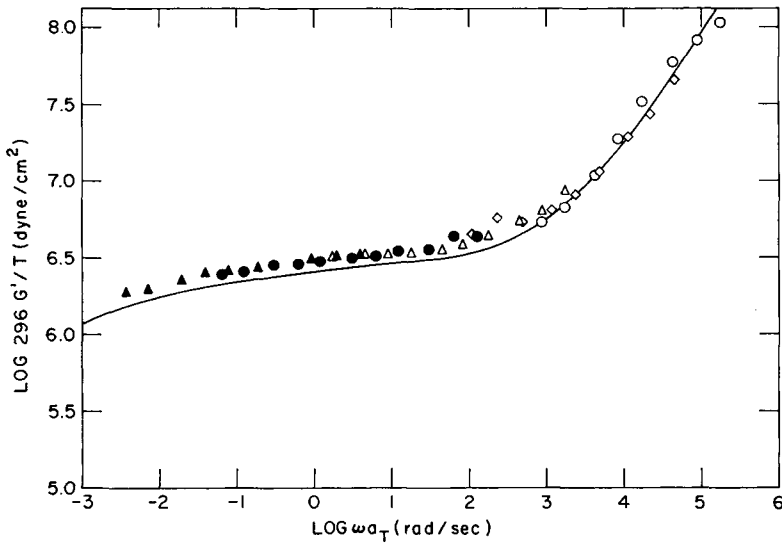


Fig. 9. Temperature-reduced storage modulus (in shear) of NBS polyisobutylene as measured by the RSI transducer (experimental points) compared with published data (solid curve).

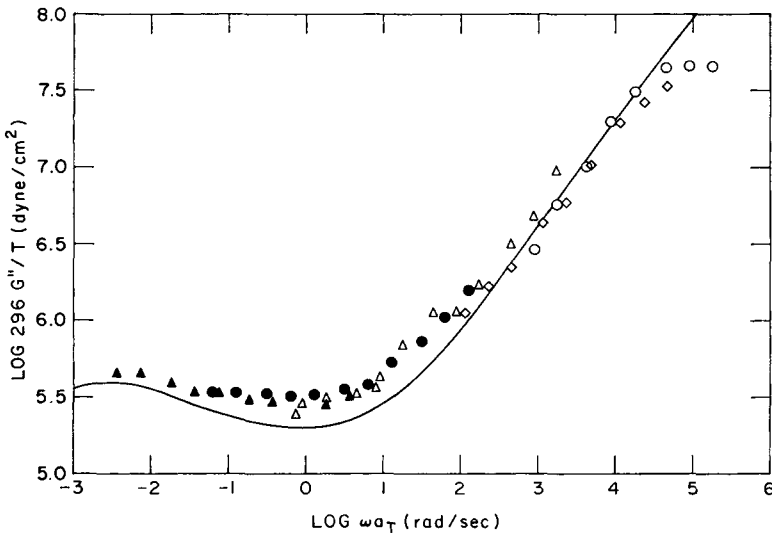


Fig. 10. Temperature-reduced modulus (in shear) of NBS polyisobutylene as measured by the RSI transducer (experimental points) compared with published data (solid curve).

Figures 9 and 10 are typical of many examples of successful data correlation between RSI results and other dynamic (by Fitzgerald transducer)¹¹⁻¹³ and static (stress relaxation)^{13,14} measurements on a wide variety of polymers. The RSI transducer and instrumentation described in this report are restricted to the shear moduli range from 10^5 to 10^8 dynes/cm². This range may be extended by modified transducer design and attention is currently addressed to providing a broadened range of measurement.

DISCUSSION

The RSI transducer and the associated instrumentation described here have been in operation in our laboratories for several years. In this time a large variety of soft viscoelastic polymers have been analyzed with regard to their dynamic properties. In this sense, the RSI method is comparable to other established methods of obtaining dynamic data.

The only special restriction of the RSI method, as the theory has already pointed out, results from the fact that instantaneous stress and strain are not homogeneous over the spherical area of shear. This inhomogeneity of shear stress and strain makes evaluation of nonlinear viscoelastic response more difficult to assess. The presence of nonlinearity, is, however, easily detected by a dependence of $G'(\omega)$ upon ΔX_t . The simplified theory presented here assumes linear viscoelasticity and normally in the response region for 10^5 to 10^8 dynes/cm² this result is realized with high molecular weight elastomers at low shear strain where $\gamma \leq \pm 0.1$.

Perhaps the unique feature of the RSI method is the extreme range of very low dynamic frequency, from 0.001 to 44 cycles, made available by the rotational generator. Standard methods¹¹⁻¹³ of dynamic measurement operate in the acoustical frequency range from 25 to 10,000 cycles/sec. This low frequency range of the RSI method provides a unique capability to examine the rubbery plateau and entanglement slippage regions of viscoelastic response without the need for extensive superposition of data by time-temperature reduction. The only practical limit to low frequency by the rotational measurement is the patience of the operator. In ordinary circumstances of measurement, 0.01 cycle/sec is the lowest frequency employed in our work.

Another basic feature of the RSI method is the fact that under steady state conditions of measurement no element of the instrument except the sample is undergoing oscillatory motion. Furthermore, the forces F_1 and F_2 are static components of a dynamic response of the sample and any fluctuation in their values can be traced to spherical asymmetry. This latter fact permits the force measurement by a simple yet precise and sensitive system such as provided by the Instron circuitry.

As previously mentioned in the discussion of instrumentation, the RSI transducer is interchangeable with a standard Maxwell-type specimen. Combining the two capabilities for dynamic measurement in a single apparatus provides an almost unparalleled versatility. The addition of

the rotational accessory, shown in Figure 6, with the well-known capability of the Instron for transient and static measurements, provides an outstanding range of use in a single equippage. Experience has shown that the rotational accessory does not interfere with the ordinary use of the Instron.

The Instron rotational accessory is not necessarily limited to RSI or standard Maxwell beam measurements. The apparatus illustrated in Figures 7 through 9, by minor mechanical modifications, could measure rotational shear properties of elastomers by the rotating cylinder method described by Gent.¹⁵ Addition of a vertical load-measuring axis would equip this accessory to measure rotational shear properties of polymer melts by the orthogonal rheometer method of Maxwell and Chartoff.¹⁶⁻¹⁹

The writer gratefully acknowledges the assistance of Messrs. R. F. Huberty, R. S. Reylek, J. T. Rueb, and E. G. Saari during the period of instrument development. The author additionally wishes to gratefully acknowledge the referee's contribution in providing a correction in eq. (11) of this derivation.

References

1. B. Maxwell, *J. Polym. Sci.*, **20**, 551 (1956).
2. B. Maxwell, *ASTM Bull.*, No. **215**, 76 (July 1956).
3. D. H. Kaelble, *J. Appl. Polym. Sci.*, **9**, 1201 (1965).
4. D. H. Kaelble, *SPEJ.*, **15**, 1071 (1959); *J. Appl. Polym. Sci.*, **9**, 1213 (1964).
5. D. H. Kaelble, *J. Appl. Polym. Sci.*, **9**, 1209 (1965).
6. D. H. Kaelble, in *Treatise on Adhesion and Adhesives*, Vol. 1, R. L. Patrick, Ed., Marcel Dekker, New York, 1967, chapter 5.
7. R. S. Marvin, in *Proc. Second International Congress Rheology*, Butterworth, London, 1954, p. 156.
8. C. A. Dahlquist and M. R. Hatfield, *J. Coll. Sci.*, **7**, 253 (1953).
9. W. R. Krigbaum and P. J. Flory, *J. Amer. Chem. Soc.*, **75**, 1775 (1953).
10. M. I. Williams, R. F. Landel, and J. D. Ferry, *J. Amer. Chem. Soc.*, **77**, 3701 (1955).
11. E. R. Fitzgerald, *Phys. Rev.*, **108**, 690 (1957).
12. E. R. Fitzgerald and J. D. Ferry, *J. Coll. Sci.*, **8**, 1 (1953).
13. J. D. Ferry, *Viscoelastic Properties of Polymers*, Wiley, New York, 1961, Chapter 6.
14. A. V. Tobolsky, *Properties and Structure of Polymers*, Wiley, New York, 1960.
15. A. N. Gent, *Brit. J. Appl. Phys.*, **11**, 165 (1960).
16. B. Maxwell and R. P. Chartoff, *Trans. Soc. Rheol.*, **9**, 41 (1965).
17. L. L. Blyler, Jr., and S. J. Kurtz, *J. Appl. Polym. Sci.*, **11**, 127 (1967).
18. R. B. Bird and E. K. Harris, *A.I.Ch.E. J.*, **14**, 758 (1968).
19. B. Maxwell *Polym. Eng. Sci.*, **7**, 145 (July 1967); **8**, 252 (Oct. 1968).

Received July 14, 1969

Revised August 8, 1969